ISIJ International, Vol. 61 (2021), No. 7, pp. 2092–2099
https://doi.org/10.2355/isijinternational.ISIJINT-2021-037

Evaluation of Thermodynamic Driving Force and Effective Viscosity of Secondary Steelmaking Slags on the Dissolution of Al_2O_3-Based Inclusions from Liquid Steel

Pedro CUNHA ALVES, Vinicius CARDOSO DA ROCHA, Julio Aníbal MORALES PEREIRA, Wagner Viana BIELEFELDT* and Antônio Cezar Faria VILELA

Department of Metallurgy (DEMET), Federal University of Rio Grande do Sul (UFRGS), Porto Alegre, Brazil.

(*Received on January 29, 2021; accepted on March 19, 2021*)

Dissolution of Al_2O_3-based inclusions are paramount during production of special steel and slag engineering is key to enhance this phenomenon. This work evaluates the influence of thermodynamic driving force (ΔC) and effective viscosity (η_e) on steel cleanliness of three distinct steel grades and slag composition (Steel/Slag A, Steel/Slag B and Steel/Slag C). Initial and final steel and slag samples were withdrawal on an electric steelmaking facility. The first samples after addition of aluminum as deoxidizer and the second after vacuum degassing stage. X-ray fluorescence and optical spectrometry obtained initial and final samples chemical composition. An ASPEX Explorer acquired inclusions data and FactSage v.7.2 performed thermodynamic calculations. Analysis of steel Al and O content highlighted an inefficient dissolution of Al_2O_3-based inclusions for Steel/Slag A, deteriorating steel cleanliness. Furthermore, this phenomenon is supported by average inclusions composition on initial and final samples plotted in pseudo-ternary diagram. Steel/Slag B and C provided improved results regarding the dissolution of Al_2O_3-based inclusions with a final inclusion density below 0.50 mm^{-2}. These two slags composition achieved values of ΔC above 25 and η_e close to 0.10 Pa·s. In addition, their combined effect ($\Delta C/\eta_e$) presented values above 250 and had the highest linear fit among these analyses. These properties are influenced by slags chemical composition and can be improved controlling parameters as binary basicity and CaO/Al_2O_3 ratio. Slags B and C were selected to define an optimal range for these parameters, with binary basicity between 3.00–3.50 and CaO/Al_2O_3 ratio in a range from 2.50–3.50.

KEY WORDS: FactSage; refining slags; Non-metallic inclusions; effective viscosity.

1. Introduction

After primary refining, liquid steel presents elevated total oxygen (T.O.) values due to the oxidizing characteristic of this stage during steel production.[1–3] The liquid steel is submitted to deoxidation process during the tapping process in order to decrease total oxygen content. At this moment, numerous inclusions are formed in liquid steel as the result of reactions between dissolved oxygen and metallic alloys added as deoxidizer.[4,5] These inclusions must be removed to obtain a higher level of steel cleanliness, with this process being one of the main functions of secondary refining slags.[6,7] The removal of inclusions occurs in three steps: flotation, separation, and dissolution.[7–10] Moreover, slag liquid fraction is considered the portion that effectively reacts with inclusions, leading to their dissolution from liquid steel.[9–12] In most cases, only ladle metallurgy is not enough to achieve the desired properties related to steel cleanliness. Thus, the steel is also submitted to vacuum degassing before the continuous casting process, increasing its cleanliness.[13–15]

Aluminum is one of the most common deoxidizers, being responsible to profoundly decrease dissolved oxygen on liquid steel. This effect is mainly explained by the thermodynamic equilibrium between soluble aluminum (Al) and oxygen (O).[4,16,17] After addition of aluminum as deoxidizer, formation of alumina clusters is first observed and subsequently the formation of spinel ($MgO{\cdot}Al_2O_3$) takes place.[4,18,19] Lastly, oxides inclusions in $CaO–Al_2O_3–MgO$ system are the most common type found after the deoxidation process. These Al_2O_3-based inclusions should be removed from liquid steel and this process is commonly affected by slag properties such as the thermodynamic driving force (ΔC) and effective viscosity (η_e).[7,10,12,20,21]

Thermodynamic driving force (ΔC) has been studied in the past years in order to understand its effect on the dissolution

* Corresponding author: E-mail: wagner@ct.ufrgs.br

of Al_2O_3-based inclusions (Al_2O_3 and $MgO{\cdot}Al_2O_3$).[7,10,20] Once the dissolution of these inclusions is controlled by mass transfer, the difference between the Al_2O_3 wt.% of the interface and the bulk (ΔC) have a significant influence in this process. In general, an increase in this property leads to a higher efficiency of inclusions dissolution.[7,10,20] In the other hand, slag viscosity is also paramount for the process of inclusion removal. This property includes slags solid and liquid fraction and shows up as an efficient tool to evaluate steel cleanliness.[12,21]

Thermodynamic software such as FactSage[22] and Thermocalc[23] are excellent tools to calculate viscosity of liquid slags. It is important to note that steelmaking slags have both a liquid and a solid fraction, prompting some additional steps to obtain effective viscosity using these programs. In order to surpass this characteristic, Roscoe-Einstein[24] equation can be used to calculate effective viscosity for steelmaking slags.[12,21,25] Output information from thermodynamic software as liquid fraction and liquid viscosity are used on this equation in order to obtain the effective viscosity of steelmaking slags. This property seems to be highly influenced by slag liquid fraction,[21] which is also the fraction that interacts with liquid steel promoting reactions like inclusion dissolution.[9–12] Thus, understand the influence of effective viscosity in steel cleanliness is crucial for the production of special steels.

The objective of this work was to analyze the influence of thermodynamic driving force (ΔC) and effective viscosity (η_e) of secondary steelmaking slags on the dissolution of Al_2O_3-based inclusions. Therefore, properties such as inclusion density, area fraction, and total oxygen content were used for this evaluation. Lastly, thermodynamic and physical slag properties as ΔC and η_e were analyzed to define an optimized slag composition focused on the following parameters: binary basicity and CaO/Al_2O_3 ratio.

2. Materials and Methods

Twenty-one heats from an electric steel mill were selected for this study. These heats include three different steel grades with an average carbon content of 0.37, 0.52, and 0.99 wt.%. Therefore, steel and slag samples were separated into groups A, B, and C in further analyses. The final application of these steel grades are the automotive industry, which demands a high level of cleanliness.[26,27] The analyses of three different steel grades with different slags practices allowed an extensive range of slag composition, being possible to better evaluate their influence on thermodynamic driving force and effective viscosity. Samples of steel and slag were taken before and after vacuum degassing, with initial samples collected after the deoxidation process and adjust of slag and liquid steel. After these processes, liquid steel was submitted to vacuum degassing to improve steel cleanliness, and therefore final samples were collected. **Figure 1** presents the steelmaking route of the existing industrial plant with sample withdrawal locations.

The process starts with the melting of metallic load in an Electric Arc Furnace (EAF). After primary refining, liquid steel is submitted to secondary refining with a vacuum degassing (<150 Pa) stage. This steelmaking plant operates a ladle with a volume of 8.9 m^3, totalizing an average amount of 62 t of liquid steel per heat. The stirring process with Argon gas is performed through one porous plug in the center of the ladle, presenting an average flow rate of 125 Nl/min. The average temperature during the secondary refining is 1 600 °C, which was the chosen value for thermodynamic calculations. The solidification process occurs in a continuous casting equipment.

Steel samples were withdrawal using Sample-O-Line (from Heraeus Electro-Nite) without the presence of deoxidizer. Steel chemical composition and total oxygen content were measured with an ARL 3560 Optical Emission Spectrometer and LECO TC-436 equipment, respectively. Slags chemical composition was determined by X-ray fluorescence (XRF) using a Philips PW2600 equipment. Their values were normalized to the $CaO–SiO_2–Al_2O_3–MgO$ oxide system because of its great importance during secondary refining.[28] The sum of these oxides was above 95% in original compositions.

For inclusion analyses, an ASPEX Explorer was used and the analyzed area varied between 54.3 to 83.7 mm^2. Output data from this equipment was applied in an MS Excel spreadsheet developed at Ironmaking and Steelmaking Laboratory. Other authors[10,12,28,29] had used this spreadsheet in their works, and its functions are described in their following papers. Chemical composition, size distribution, and inclusion classification were obtained; with all this information being paramount to evaluate steel cleanliness.[30,31] Pure alumina, spinel, calcium aluminates, and $CaO–MgO–Al_2O_3–SiO_2$ oxide inclusions were defined as Al_2O_3 based-inclusions and selected to further analyses. Inclusions chemical composition was plotted in ternary

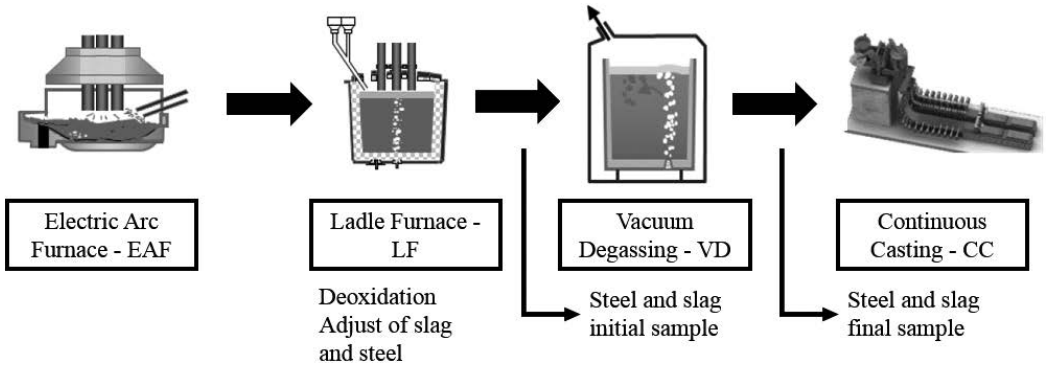

Fig. 1. Steelmaking route and withdrawal moments of steel and slag samples.

diagram using software RStudio v.3.5.1 with *ggplot2* and *ggtern* package.[32,33]

Thermodynamic calculations were performed using commercial software FactSage v.7.2 at a temperature of 1 600°C and pressure of 1 atm. Initial slags chemical composition was plotted in $CaO–Al_2O_3–SiO_2–MgO$ ternary diagram using Phase Diagram module and *FToxid* and *FactPS* databases. Slags chemical composition was also analyzed concerning their liquid and solid fraction, and liquid fraction chemical composition using *Equilib* module.

Regarding the dissolution of alumina inclusions, it is possible to analyze the contribution originated from the difference between Al_2O_3 wt.% from the interface and the bulk. The bulk wt.% is represented as the alumina content in slag liquid fraction, and the interface wt.% is inferred as the Al_2O_3 saturation point.[10,34–36] Thus, the thermodynamic alumina driving force (ΔC) was calculated, as shown in Eq. (1).

$$\Delta C = \left(Al_2O_3\right)_{sat} - \left(Al_2O_3\right)_{bulk} \quad \text{..... (1)}$$

Al_2O_3 saturation point was calculated using the liquid fraction chemical composition obtained in previous steps. The input data used in *Equilib* module at FactSage is demonstrated in **Table 1**. Al_2O_3 weight percent was set as <A>, with this value varying from 0 to 60 with increments of 1. Every time a new phase is formed, the program indicates the correspondent <A> value.[22] Once the new phase formed presents Al_2O_3 as a component, the saturation point is achieved. Spinel and calcium aluminates are examples of alumina-saturated phases.[7,34,35,37]

Lastly, the *Viscosity* module with *Melts* database was used to calculate viscosity (η) of slags liquid fraction. Roscoe-Einstein's model,[24] Eq. (2), was applied to obtain slags effective viscosity (η_e), which takes into account slags solid fraction (c).

$$\eta_e = \eta\left(1-c\right)^{-2.5} \quad \text{..... (2)}$$

Table 1. FactSage input data for slag oxides.

Slag oxide	Weight percent (wt.%)
Al_2O_3	<A>
SiO_2	<(100 – MgO – A)/(B_2^a+1)>
CaO	<B_2^a(100 – MgO – A)/(B_2^a+1)>
MgO	MgO[b]

[a]B_2 = Binary basicity; [b]Chemical composition value.

3. Results and Discussion

3.1. Steel Chemical Composition and Inclusion Analysis

Initial and final steel chemical composition were separated into three groups (A, B, and C) and presented in **Table 2**. Steel A, B, and C are modified special steels DIN38MnS, SAE1050, and SAE52100, respectively. The average composition, weight percent or ppm depending on the element, was presented for each group with its correspondently standard deviation (σ).

In general, a lower standard deviation was visualized for the analyzed elements, indicating a stability on the process. Steel A presents the highest Si and Mn values, perhaps due to the usage of these elements as the main deoxidizers during the tapping with following addition of aluminum to complete deoxidation process. Si and Mn are considered weak deoxidizers, presenting high values of soluble oxygen in equilibrium.[17] As a result, Steel A has the highest total oxygen values observed for both initial and final samples between all steel grades. Steel A also presents the highest Al values, which should have decreased total oxygen content due to equilibrium conditions between Al and O. A possible explanation is that the addition of aluminum as deoxidizer decreased soluble oxygen, however the dissolution of Al_2O_3-based inclusions (deoxidation product) did not occur properly, maintain a significant amount of oxygen in form of oxide on liquid steel. Since T.O. is the sum of soluble and oxide oxygen,[38] an increased level of Al_2O_3-based inclusions will contribute to keep this value elevated. The lowest values of T.O. are observed on Steel B and C, which also present similar values of total Al compared to Steel A. These results indicate that Steel B and C had a better inclusion removal than Steel A, lowering the oxide oxygen and consequently the T.O. on samples. For the other elements, calcium did not present a variation between groups. Concerning sulfur, except for steel A (resulfurized steel grade), it is observed a decrease in its content. Nitrogen has the same behavior for all groups, with a reduction from initial to final samples.

Inclusion population was analyzed in relation to the following properties: inclusion density, area fraction, and average diameter. **Figure 2** summarizes Al_2O_3-based inclusions results for initial and final steel samples. Total oxygen variation is also presented because of its importance as an indirect measure of steel cleanliness.[39]

Inclusion density (Fig. 2(a)) and area fraction (Fig. 2(b))

Table 2. Steel chemical composition and standard deviation (σ).

Steel	Sample	C (wt.%)	σ	Si (wt.%)	σ	Mn (wt.%)	σ	Al (ppm)	σ	Ca (ppm)	σ	S (ppm)	σ	N (ppm)	σ	T.O.[a] (ppm)	σ
A	Initial	0.34	0.02	0.57	0.03	1.28	0.06	49	4	7	2	166	36	151	37	64	29
	Final	0.37	0.01	0.63	0.02	1.14	0.07	69	27	7	3	397	36	110	31	27	13
B	Initial	0.50	0.01	0.22	0.02	0.60	0.03	38	13	7	2	196	46	92	7	51	20
	Final	0.52	0.01	0.24	0.01	0.75	0.01	35	4	5	1	130	31	63	14	17	4
C	Initial	0.94	0.03	0.25	0.03	0.21	0.03	37	11	6	2	90	29	111	15	28	5
	Final	0.99	0.02	0.25	0.02	0.31	0.02	40	12	5	3	39	21	66	5	14	4

[a]Total oxygen

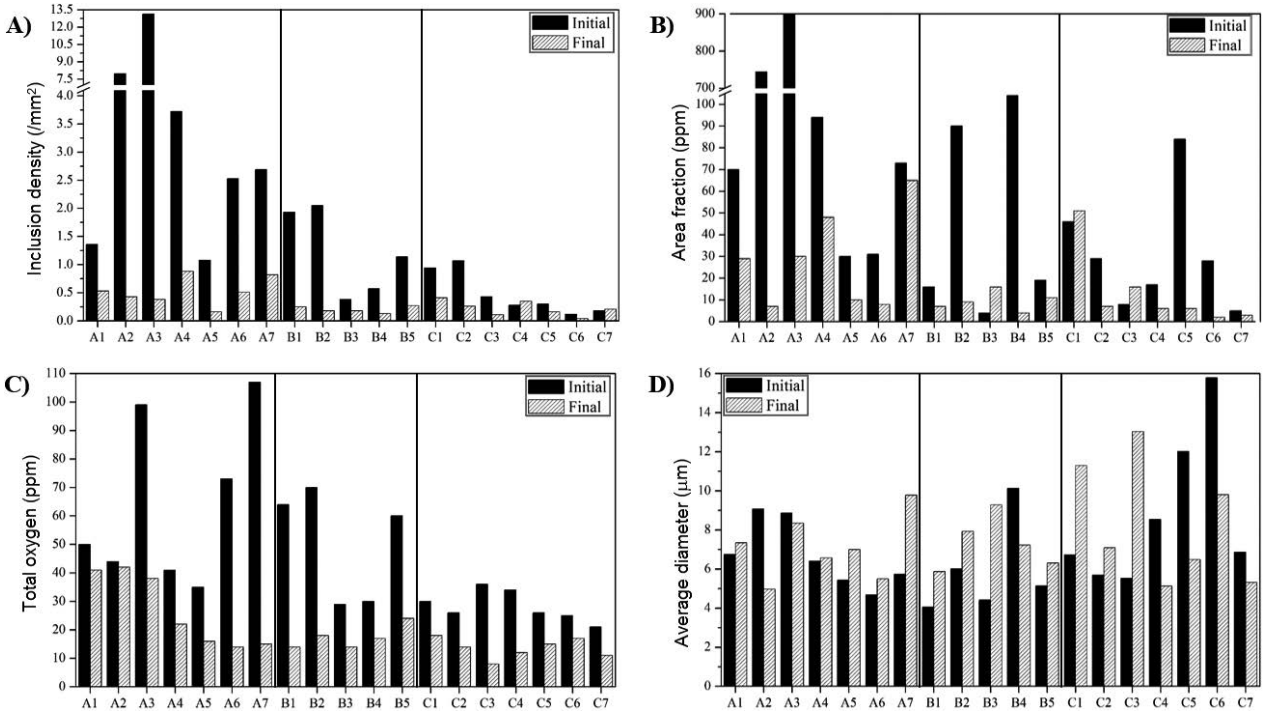

Fig. 2. Inclusion analysis summarized. (a) Inclusion density; (b) Area fraction; (c) Total oxygen; (d) Average diameter.

presented similar patterns, with highest values observed for Steel A. These results match with previous statement that Steel A did not show a properly dissolution of Al_2O_3-based inclusions. In general, for all steel grades there is a decrease in inclusion density and area fraction from initial to final sample. These results follow previous literature, where other authors also verified a pronounced removal of inclusions during vacuum degassing, lowering values of inclusion density and area fraction.[13–15] Three heats (B3, C1 and C3) did not present a decrease on area fraction and this result can be explained by a possible coalescence of inclusions during vacuum degassing.[13] A slight increase in the average diameter of inclusions is observed for all steel grades, including samples B3, C1 and C3, corroborating the hypothesis of inclusion coalescence during vacuum degassing for these heats. The average diameter observed in the final sample are classified as micro inclusions (dia. < 11.5 μm), according to Capurro *et al.*[13] In addition, Kong *et al.*[40] also found similar diameter for Al_2O_3-based inclusions after vacuum degassing. This classification affects the evaluation of cleanliness and steel final application since macro inclusions could lead to failure at the beginning of operation.[17,27] Lastly, T.O. declined on all final samples, matching with inclusion population results described on this section and previous literature.[2,13,15,17]

Upcoming analyses use inclusion density as a steel cleanliness parameter. However, area fraction plays an important role and needs to be evaluated as well.[26] **Figure 3** presents a correlation between these properties.

The result is a tendency where lower values of area fraction are correlated with lower inclusion density. This pattern supports the subsequent usage of inclusion density since the same is linked to area fraction, with similar behaviors between then.

Inclusions were analyzed under the viewpoint of density, area fraction, and average diameter. Afterward, chemical

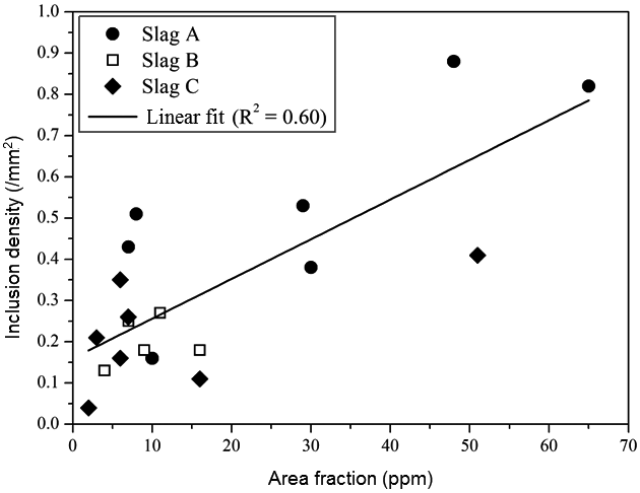

Fig. 3. Correlation between inclusion density and area fraction in the final samples.

composition of inclusions was plotted in $CaO–MgO–Al_2O_3$ and $CaO–Al_2O_3–SiO_2$ ternary diagrams. All inclusions of each steel grade were plotted together on the same ternary diagram, providing a complete and dynamic view of the average chemical composition behavior on initial and final samples. Density function of *ggtern* package organized and plotted the date as contour lines and **Fig. 4** summarizes the result. The density function provides an insightful view about the behavior of inclusion for each steel grade. However, the authors were not able to provide an appropriate label for the different color intensity. This is a limitation of *ggtern* package that the authors were not able to surpass. A correct interpretation of Fig. 4 shows that areas in black concentrates a higher number of inclusions compared to grey areas.

Steel A (Fig. 4(a)) has the majority of inclusions classified as calcium aluminates (solid and liquid) and oxides

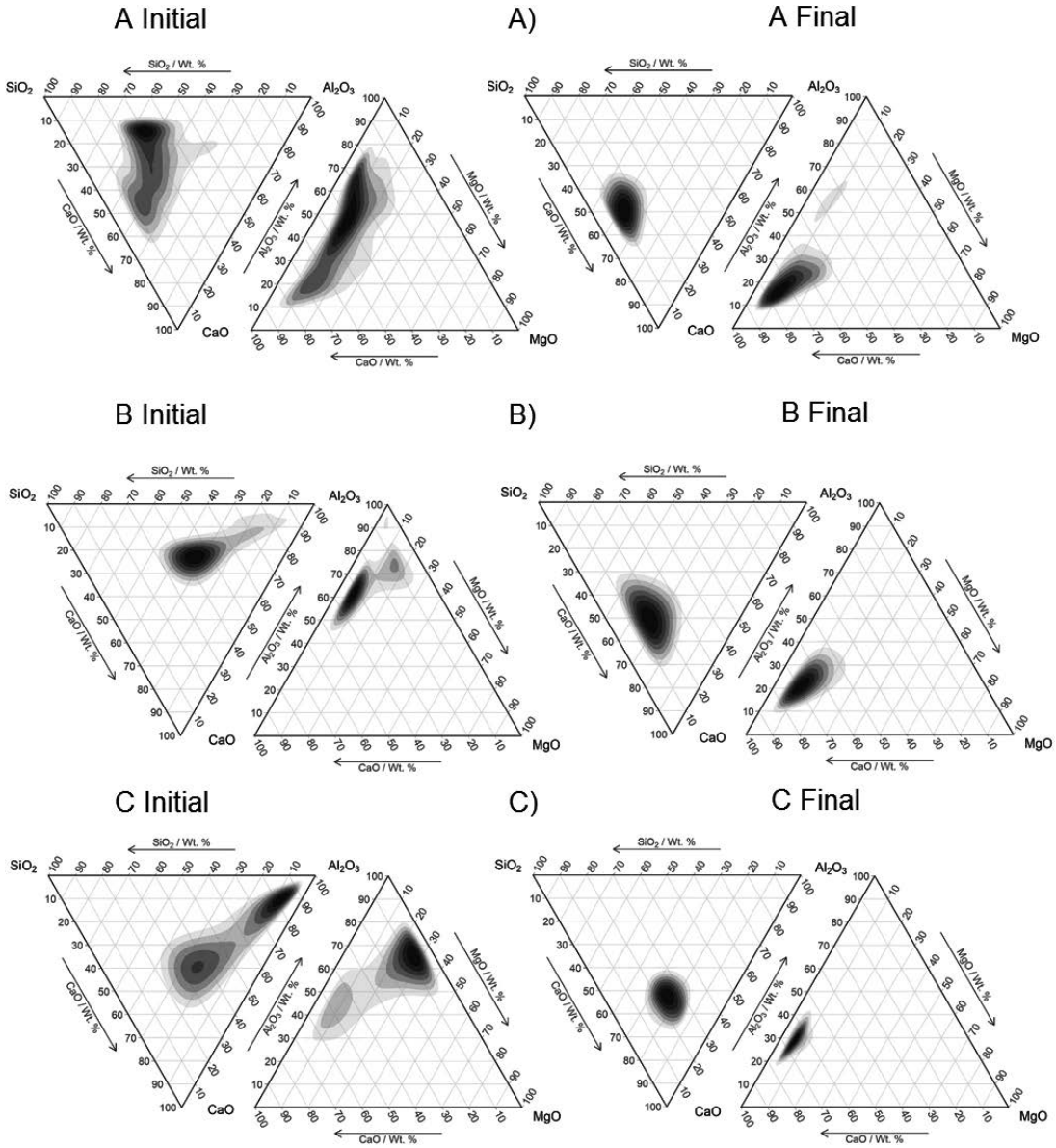

Fig. 4. Inclusions average chemical composition on initial and final steel samples as contour lines plotted in CaO–Al_2O_3–SiO_2 and CaO–MgO–Al_2O_3 ternary diagram (a) Steel A; (b) Steel B; (c) Steel C.

in the CaO–MgO–Al_2O_3–SiO_2 system before vacuum degassing. Final sample presents a different pattern with a decrease in these Al_2O_3-based inclusions. Furthermore, oxides inclusions on final sample present a homogenous composition compared to initial sample. Steel B (Fig. 4(b)) and C (Fig. 4(c)) present different types of inclusions then Steel A. These steel grades have the presence of calcium aluminates (solid – Steel B; liquid – Steel C) along spinel as main inclusions on initial samples. After vacuum degassing, Al_2O_3-based inclusions were reduced on both steel grades, A and B. At this stage, a similar average chemical composition of inclusions is observed for all three steel grades analyzed. It is also important to note the pattern that average composition moved away from Al_2O_3 axis on all final steel sample, being a factor that supports the dissolution of Al_2O_3-based inclusions by steelmaking slags during vacuum degassing.

3.2. Slag Analysis

Average slag chemical composition, liquid fraction and standard deviation are summarized on **Table 3**. Each steel grade was produced with its own slag composition and thus they were divided as A, B, and C.

There is a minor variation on slags composition from initial to final sample. Therefore, initial composition of slags was assumed as the bottom line for reactions regarding the dissolution of inclusions. CaO wt.% increased and SiO_2 wt.% decreased from Slag A to C. These variations induced an increase in binary basicity (CaO wt.%/SiO_2 wt.%), with an average of 2.00, 2.91 and 3.61 for Slags A, B and C respectively. Al_2O_3 wt.% presented the greater variation between the analyzed oxides increasing from 10.53 wt.% in Slag A to 21.53 wt.% in Slag C. This pattern affected slag liquid fraction results. An increase in Al_2O_3 wt.% lead to an increase in liquid fraction (Slag A: 67.06%; Slag B: 76.24% Slag C: 95.73%). Regarding inclusion dissolution, slags must have a substantial liquid fraction since this is the portion that interacts with liquid steel and promotes this phenomenom.[9–12] Ultimately, C/A (CaO wt.%/Al_2O_3 wt.%) ratio decreased from Slag A to C as the result of chemical compositions variations observed.

Table 3. Average slag chemical composition, liquid fraction and standard deviation.

	Sample	CaO (wt.%)	σ	SiO_2 (wt.%)	σ	Al_2O_3 (wt.%)	σ	MgO (wt.%)	σ	FeO (wt.%)	σ	MnO (wt.%)	σ	LF[a] (%)	σ	LF minimun	LF maximum
A	Initial	49.09	3.51	24.87	2.82	10.53	2.92	13.85	1.96	1.22	0.37	0.44	0.14	67.06	17.33	48.32	93.48
	Final	46.55	4.46	26.70	1.84	10.32	3.18	14.88	2.78	1.04	0.51	0.51	0.11	71.40	20.60	48.68	94.19
B	Initial	50.72	4.01	17.41	0.33	13.88	2.79	16.27	4.14	1.43	0.27	0.29	0.10	76.24	15.24	50.16	88.77
	Final	44.24	2.24	20.94	1.53	14.63	2.77	18.92	5.93	0.89	0.28	0.38	0.05	83.69	14.50	60.56	96.00
C	Initial	52.85	2.93	15.40	3.45	21.53	3.02	9.12	1.99	0.98	0.32	0.11	0.03	95.73	1.34	93.59	97.66
	Final	50.79	1.92	16.41	1.63	20.34	3.32	11.68	2.34	0.67	0.25	0.12	0.05	93.78	3.95	85.37	96.94

[a]Liquid fraction.

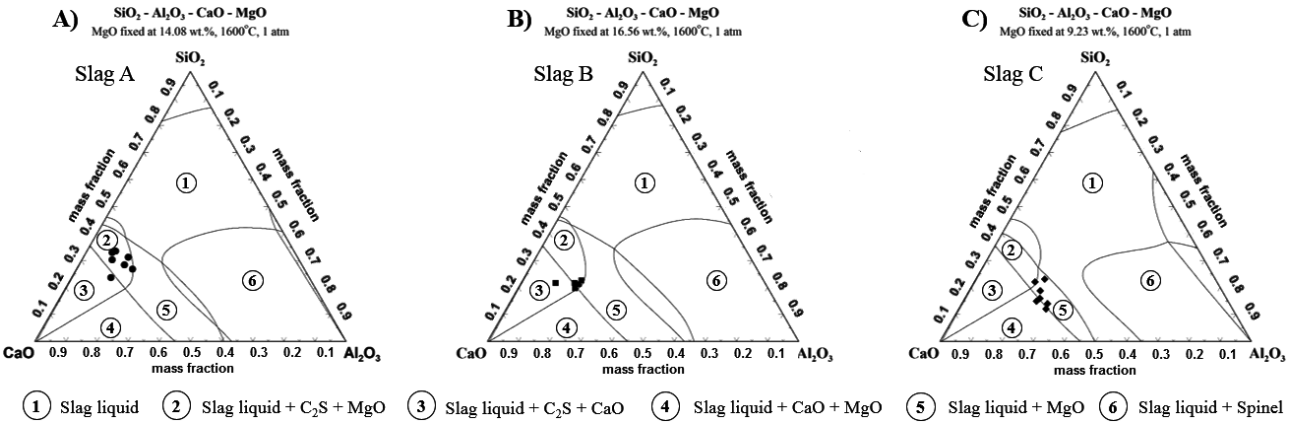

Fig. 5. Initial slag chemical composition plotted in CaO–Al_2O_3–SiO_2–MgO pseudo-ternary diagram at 1 600°C and 1 atm.

Initial chemical composition of each slag was plotted in CaO–Al_2O_3–SiO_2–MgO pseudo-ternary diagram using FactSage and the results are exposed in **Fig. 5**.

For Slag A (Fig. 5(a)), it is observed the presence of the following phases at 1 600°C: liquid slag, C_2S ($2CaO{\cdot}SiO_2$) and MgO. Slag B (Fig. 5(b)) chemical composition is located closest to region presenting only liquid slag and MgO saturation field, and consequently closer to its MgO saturation point. Lastly, Slag C (Fig. 5(c)) had its chemical composition presenting liquid slag plus MgO. Their position in the diagrams, approaching the liquid slag only area, agrees with the increased liquid fraction results verified in Table 3. With the results presented for slag chemical composition, it is possible to compare Slags A, B and C to slags used by Valdez *et al.*[7] in a previous work discussing the dissolution of Al_2O_3-based inclusions. Between our samples, Slag C presents the best composition and consequently position on the pseudo-ternary diagram for a reliable and efficient dissolution of Al_2O_3-based inclusions.[7]

Afterwards, Table 4 presents chemical composition of liquid fraction of slags along their B_2 (binary basicity: %CaO/%SiO_2) and C/A ratio. Same patterns previously observed for Al_2O_3 wt.%, binary basicity and CaO/Al_2O_3 ration in Table 3 are verified for the liquid portion of the analyzed steelmaking slags. Slags liquid fraction chemical composition can be used as target composition for inclusions since it composition approach the one observed for slag liquid fraction during secondary refining process.[1,13,14,41] This phenomenon was tested and results are expressed in **Fig. 6**. Initial and final Al_2O_3 wt.% in inclusions were compared with the Al_2O_3 wt.% present on liquid slag fraction.

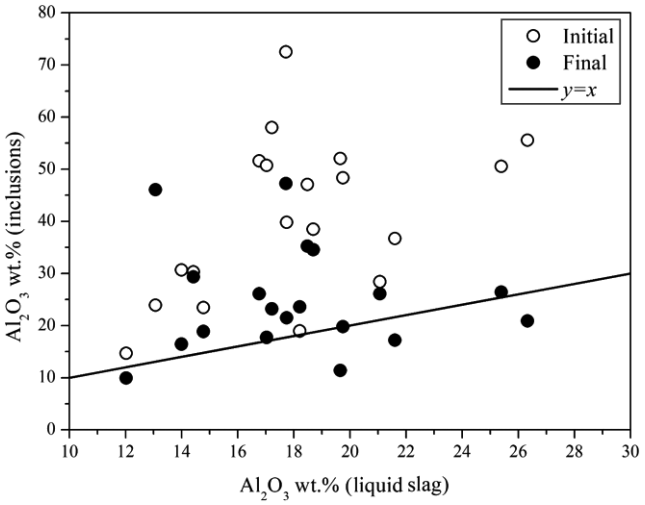

Fig. 6. Comparison between Al_2O_3 wt.% observed on chemical composition of inclusions and initial liquid slag fraction.

Figure 6 also presents a comparative line y=x to help this comparison.

Most samples presented a decrease in inclusions Al_2O_3 wt.% on final samples compared to their initial state, matching with the phenomenon explained before.

Results presented until now support an effective dissolution of Al_2O_3-based inclusions on all three steel samples. Nevertheless, each steel grade and its correspondent slag composition presented different numbers for inclusion population. Using inclusion density as the major parameter for comparison, Slag C presents the lower values for this property on final steel samples. Slags chemical composition

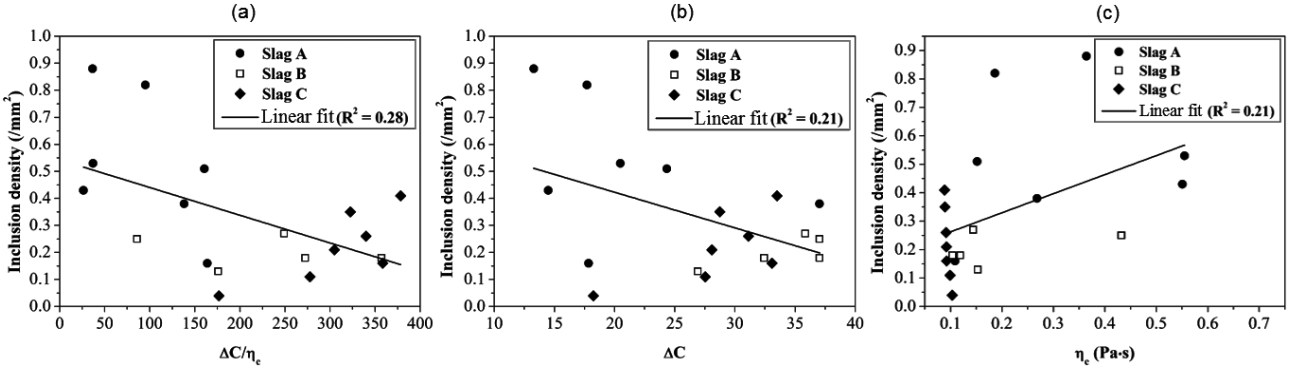

Fig. 7. Correlation between final inclusion density with thermodynamic driving force (ΔC), effective viscosity (η_e) and their combined effect ($\Delta C/\eta_e$). (a) Inclusion density vs. $\Delta C/\eta_e$; (b) Inclusion density vs. ΔC; (c) Inclusion density vs. η_e.

seem to play an important role, directly affecting results on inclusion density. Therefore, thermodynamic driving force (ΔC) and effective viscosity (η_e), properties that affect the removal and dissolution of Al_2O_3-based inclusions, surge as possible parameters to explain the different behavior observed on this work. Their combined effect ($\Delta C/\eta_e$) was also analyzed since previous works found exciting results with this methodology.[10,20,34,35] **Figure 7** summarizes these three properties and their correlation with final inclusion density.

Thermodynamic driving force and effective viscosity affect final inclusion density in a certain level. The behavior found in this work for both properties match with similar previous works that analyzed their effect on the efficiency of inclusion removal.[10,20,35] An increase in ΔC and a decrease in η_e can lead to a higher dissolution of Al_2O_3-based inclusions and consequently lower inclusion density. Regarding ΔC parameter (Fig. 7(b)), Slags B and C presented better results, with the majority of samples above 25 ΔC. In addition, these samples present an inclusion density below 0.50 mm^{-2}. On the other hand, Slag A presents only one sample below this value, and their ΔC are all below 25. This result indicates that ΔC values above 25 have a higher capability to absorb and dissolve Al_2O_3-based inclusions. For the other parameter, effective viscosity, in general it is expected that lower values would lead to a better inclusion removal.[12,14,21] This pattern is verified in Fig. 7(c), with lowest values of effective viscosity aligned with lowest values of inclusion density. Most inclusion density values below 0.50 mm^{-2} are concentrated in the region close to a η_e of 0.10 Pa·s. In addition, the majority of these samples are from Slags B and C. One more time, Slag A, with the worst results for inclusion density differed from the other two slag composition. Combining these two parameters ($\Delta C/\eta_e$) in Fig. 7(a) provided the highest linear fit between the analysis and raised as a remarkable tool to evaluate the dissolution of Al_2O_3-based inclusions. Combination of ΔC and η_e comprises the analyses of both thermodynamic and physical properties of slags, thus leading to a robust analysis on Al_2O_3-based inclusions dissolution. Results expose those values above 250 for $\Delta C/\eta_e$ lead to a decrease inclusion density. This region is responsible to compress samples with inclusion density below 0.50 mm^{-2}. As it is observed for the individual analyses, Slags B and C are observed in this area. This result also agrees with the since higher values of $\Delta C/\eta_e$ are linked to a high ΔC, low η_e or combination of both. This pattern provides a path to improve dissolution of Al_2O_3-based inclusions during secondary refining using ΔC and/or η_e as key factors on steelmaking slags.

Lastly, considering that Slags B and C presented most improved results on previous analysis in Fig. 7, their chemical composition and parameters as B_2 and C/A can help understand how to improve ΔC and η_e. For the following discussion, initial slag chemical composition (Table 3) considering both liquid and solid fraction was used. In an industrial environment, these values are easier to control than the liquid fraction composition, which needs a thermodynamic software as FactSage to be calculated. Binary basicity of average initial Slag B and C composition varies from 2.91 to 3.43 respectively. These values approached slag chemical composition to a CaO-saturated field, which is an area that can lead to a better Al_2O_3-based inclusion dissolution.[42] Regarding CaO/Al_2O_3 ratio, values alter from 3.65 (Slag B) to 2.45 (Slag C). These values are close to the ones presented by Ji *et al.*,[42] who also presented slags in the $CaO–Al_2O_3–SiO_2$ ternary diagram used by Valdez *et al.*[7] Slags with a C/A of 2.50 were located in the region with the highest ($\Delta C/\eta_e$) the same way it is observed in this present work. These results provides a window of values of improved B_2 and C/A having dissolution of Al_2O_3-based inclusions as the focus. Binary basicity ranging from 3.00–3.50 and CaO/Al_2O_3 ratio varying from 2.50–3.50 presented the better results in this work, being an optimized configuration for steelmaking slags during secondary refining. These values hang over an inclusion density below 0.50 mm^{-2}, ΔC above 25, η_e close to 0.1 Pa·s and $\Delta C/\eta_e$ above 250. In conclusion, Slags C and B have a similar final inclusion density; however, as can be seen on Fig. 3, Slag B presented a greater reduction from initial to final sample compared to Slag C. The latter already presented a lower inclusion density on initial samples, with most values below 1 mm^{-2}. This result specify Slag B with the most optimized composition, being able to dissolve a significant amount of Al_2O_3-based inclusions along a low final inclusion density below 0.50 mm^{-2}.

4. Conclusions

Concerning the dissolution of Al_2O_3-based inclusions and improvements in slags thermodynamic driving force and

effective viscosity, the following conclusions were reached:

(1) Usage of aluminum as deoxidizer without an efficient removal of inclusions lead to higher values of total Al and O. Slag A did not dissolve Al_2O_3-based inclusions properly and presented the higher values of final inclusion density ($\geq$0.50 mm^{-2}) and total oxygen (27 ppm) between slags chemical composition. Pure alumina, spinel, calcium aluminates and CaO–MgO–Al_2O_3–SiO_2 oxide inclusions were efficiently removed using these slags composition.

(2) Slags liquid fraction affected dissolution of Al_2O_3-based inclusions with Slag B (76.24%) and C (95.73%) presenting better results than Slag A (67.06%). Chemical composition of slags liquid fraction raised as an efficient tool to understand this phenomenon through the analyses of thermodynamic driving force and effective viscosity. Optimal values found for these parameters were ΔC above 25 and η_e close to 0.10 Pa·s.

(3) Combination of thermodynamic driving force and effective viscosity had a best linear fit than individual analysis. Values of $\Delta C/\eta_e$ above 250 presented superior results and this parameter can be improved throughout the control of binary basicity and CaO/Al_2O_3 ratio. Slags B and C were used to determine an optimized range of 3.00–3.50 for B_2 and 2.50–3.50 for C/A.

(4) Slags B and C presented similar results for inclusion density, total oxygen, thermodynamic driving force, effective viscosity and $\Delta C/\eta_e$. These slags were selected as target composition during the production of the steel grades for automotive industry that requires usage of aluminum as deoxidizer and subsequently dissolution of Al_2O_3-based inclusions.

REFERENCES

1) J. Björklund, M. Andersson and P. Jönsson: *Ironmaking Steelmaking*, **34** (2007), 312. https://doi.org/10.1179/174328107X168039
2) Z. Deng and M. Zhu: *ISIJ Int.*, **53** (2013), 450. https://doi.org/10.2355/isijinternational.53.450
3) L. Holappa: *J. Chem. Technol. Metall.*, **52** (2017), 159.
4) E.-I. Castro-Cedeño, M. Herrera-Trejo, M. Castro-Román, F. Castro-Uresti and M. López-Cornejo: *Metall. Mater. Trans. B*, **47** (2016), 1613. https://doi.org/10.1007/s11663-016-0640-y
5) H. L. Yang, X. L. Wu, J. S. Ye, Y. Fang and X. B. Zhao: *Ironmaking Steelmaking*, **45** (2018), 386. https://doi.org/10.1080/03019233.2016.1274549
6) R. J. Fruehan: Proc. 7th Int. Conf. on Molten Slags, Fluxes and Salts, (Cape Town), The South African Institute of Mining and Metallurgy, Johannesburg, (2004), 263.
7) M. Valdez, G. S. Shannon and S. Sridhar: *ISIJ Int.*, **46** (2006), 450. https://doi.org/10.2355/isijinternational.46.450
8) J.-H. Park, I.-H. Jung and H.-G. Lee: *ISIJ Int.*, **46** (2006), 1626. https://doi.org/10.2355/isijinternational.46.1626
9) B. H. Reis, W. V. Bielefeldt and A. C. F. Vilela: *J. Mater. Res. Technol.*, **3** (2014), 179. https://doi.org/10.1016/j.jmrt.2014.03.011
10) B. H. Reis, W. V. Bielefeldt and A. C. F. Vilela: *ISIJ Int.*, **54** (2014), 1584. https://doi.org/10.2355/isijinternational.54.1584
11) P. Rocabois, J. Lehmann, C. Gatellier and J. P. Teres: *Ironmaking Steelmaking*, **30** (2003), 95. https://doi.org/10.1179/030192303225001775
12) V. C. da Rocha, J. A. M. Pereira, A. Yoshioka, W. V. Bielefeldt and A. C. F. Vilela: *Metall. Mater. Trans. B*, **48** (2017), 1423. https://doi.org/10.1007/s11663-017-0935-7
13) C. Capurro, G. Cerrutti and C. Cicutti: Proc. 9th Int. Conf. on Clean Steel, (Budapest), Hungarian Mining and Metallurgical Society, Dunaújváros, Hungary, (2015), 1.
14) V. C. da Rocha, J. A. M. Pereira, A. Yoshioka, W. V. Bielefeldt and A. C. F. Vilela: *Mat. Res.*, **20** (2017), 1480. https://doi.org/10.1590/1980-5373-MR-2017-0188
15) K. Riyahimalayeri, P. Ölund and M. Selleby: *Ironmaking Steelmaking*, **40** (2013), 470. https://doi.org/10.1179/174328113X13711140547880
16) Z. Deng, L. Kong, D. Liang and M. Zhu: *Steel Res. Int.*, **90** (2019), 1800480. https://doi.org/10.1002/srin.201800480
17) C. Gu, Y.-P. Bao, P. Gan, J.-H. Lian and S. Münstermann: *Steel Res. Int.*, **89** (2018), 1800129. https://doi.org/10.1002/srin.201800129
18) H. Todoroki and K. Mizuno: *ISIJ Int.*, **44** (2004), 1350. https://doi.org/10.2355/isijinternational.44.1350
19) X. Deng, C. Ji, S. Guan, L. Wang, J. Xu, Z. Tian and Y. Cui: *Ironmaking Steelmaking*, **46** (2019), 522. https://doi.org/10.1080/03019233.2018.1428420
20) J. S. Park and J. H. Park: *Metall. Mater. Trans. B*, **47** (2016), 3225. https://doi.org/10.1007/s11663-016-0789-4
21) J. A. M. Pereira, V. C. da Rocha, A. Yoshioka, W. V. Bielefeldt and A. C. F. Vilela: *Mat. Res.*, **21** (2018), e20180296. https://doi.org/10.1590/1980-5373-MR-2018-0296
22) C. W. Bale, E. Bélisle, P. Chartrand, S. A. Decterov, G. Eriksson, A. E. Gheribi, K. Hack, I. H. Jung, Y. B. Kang, J. Melançon, A. D. Pelton, S. Petersen, C. Robelin, J. Sangster, P. Spencer and M. A. Van Ende: *Calphad*, **54** (2016), 35. https://doi.org/10.1016/j.calphad.2016.05.002
23) A. Costa e Silva: *J. Mater. Res. Technol.*, **1** (2012), 154. https://doi.org/10.1016/S2238-7854(12)70027-3
24) R. Roscoe: *Br. J. Appl. Phys.*, **3** (1952), 267. https://doi.org/10.1088/0508-3443/3/8/306
25) X. Li, L. Wang, S. Yang and C. Zhuang: *Ironmaking Steelmaking*, **46** (2019), 416. https://doi.org/10.1080/03019233.2018.1518808
26) E. B. Pretorius, H. G. Oltmann and B. T. Schart: Proc. AISTech 2013, (Pittsburgh), Association for Iron and Steel Technology, Warrendale, PA, (2013), 993.
27) A. Costa e Silva: *J. Mater. Res. Technol.*, **8** (2019), 2408. https://doi.org/10.1016/j.jmrt.2019.01.009
28) W. V. Bielefeldt, A. C. F. Vilela and N. C. Heck: Proc. AISTech 2014, (Indianapolis), Association for Iron and Steel Technology, Warrendale, PA, (2014), 1433.
29) P. C. Alves, J. A. M. Pereira, V. C. da Rocha, W. V. Bielefeldt and A. C. F. Vilela: *Steel Res. Int.*, **89** (2018), 1800248. https://doi.org/10.1002/srin.201800248
30) S. K. Michelic, G. Wieser and C. Bernhard: *ISIJ Int.*, **51** (2011), 769. https://doi.org/10.2355/isijinternational.51.769
31) D. Tang, M. E. Ferreira and P. C. Pistorius: *Microsc. Microanal.*, **23** (2017), 1082. https://doi.org/10.1017/S1431927617012648
32) H. Wickham: ggplot2: Elegant Graphics for Data Analysis, Springer, Cham, (2016), 1.
33) N. E. Hamilton and M. Ferry: *J. Stat. Softw.*, **87** (2018), 1. https://doi.org/10.18637/jss.v087.c03
34) J.-Y. Choi, H.-G. Lee and J.-S. Kim: *ISIJ Int.*, **42** (2002), 852. https://doi.org/10.2355/isijinternational.42.852
35) M. Valdez, K. Prapakorn, A. W. Cramb and S. Sridhar: *Ironmaking Steelmaking*, **29** (2002), 47. https://doi.org/10.1179/030192302225001965
36) W. D. Cho and P. Fan: *ISIJ Int.*, **44** (2004), 229. https://doi.org/10.2355/isijinternational.44.229
37) K. H. Sandhage and G. J. Yurek: *J. Am. Ceram. Soc.*, **73** (1990), 3643. https://doi.org/10.1111/j.1151-2916.1990.tb04270.x
38) L. Zhang and B. G. Thomas: *ISIJ Int.*, **43** (2003), 271. https://doi.org/10.2355/isijinternational.43.271
39) L. Zhang: *J. Iron Steel Res. Int.*, **13** (2006), 1. https://doi.org/10.1016/S1006-706X(06)60067-8
40) L. Kong, Z. Deng and M. Zhu: *ISIJ Int.*, **57** (2017), 1537. https://doi.org/10.2355/isijinternational.ISIJINT-2017-118
41) K. Steneholm, M. Andersson and P. Jönsson: *Steel Res. Int.*, **77** (2006), 392. https://doi.org/10.1002/srin.200606404
42) Y. Ji, C. Liu, Y. Lu, H. Yu, F. Huang and X. Wang: *Metall. Mater. Trans. B*, **49** (2018), 3127. https://doi.org/10.1007/s11663-018-1397-2